DOI: 10.1002/chem.200701500

Grafting and Thermal Stripping of Organo-Bimetallic Clusters on Au Surfaces: Toward Controlled Co/Ru Aggregates

Ahmed Naitabdi,[a] Olivier Toulemonde,[a] Jean Pierre Bucher,*[a] Jacky Rosé,[b] Pierre Braunstein,*[b] Richard Welter,[c] and Marc Drillon[a]

Dedicated to Professor W. A. Herrmann on the occasion of his 60th birthday

Abstract: The controlled stoichiometry of heterometallic carbonyl clusters make them attractive precursors for the stabilization of bare metal alloy clusters for magnetic applications. The mixed-metal molecular cluster $[RuCo_3(H)(CO)_{12}]$ has been functionalized with the phosphane–thiol ligand $Ph_2PCH_2CH_2SH$ to allow subsequent anchoring on a gold surface. The resulting tetrahedral cluster $[RuCo_3(H)(CO)_{11}(Ph_2PCH_2CH_2SH)]$ (**1**) has been characterized by X-ray diffraction and the P-monodentate ligand is axially bound to a cobalt center and *trans* to the ruthenium cap. This synthesis also yielded the product of oxidative coupling, in which two SH groups were coupled intermolecularly to give a disulfide ligand that links two tetrahedral cluster units in $[\{RuCo_3(H)(CO)_{11}(Ph_2PCH_2CH_2S)\}_2]$ (**2**). This cluster has also been characterized by X-ray diffractions studies. After deposition of **1** on a Au(111) surface by self-assembly, the carbonyl ligands were stripped off by thermal annealing in ultra-high vacuum (UHV) to form a metallic species. X-ray photoelectron spectroscopic measurements performed as a function of the annealing temperature show that the cobalt and ruthenium centers converge towards metallic character and that the stoichiometry of the alloy is retained during the annealing process. Preliminary X-ray absorption spectroscopy (XAS) synchrotron experiments indicate that clusters **1** and **2** behave similarly, which is consistent with the retention of their tetrahedral units on the gold surface after transformation of the thiol function or breaking of the disulfide bond to form Au–S bonds, respectively, has occurred.

Keywords: cluster compounds · gold · self-assembly · surface tunneling microscopy · photoelectron spectroscopy

Introduction

One of the main objectives in the field of high-density recording media is the development of microscopically controlled nanoparticles and nanostructured magnetic materials involving binary clusters or binary cluster–substrate interfaces with the highest possible intrinsic magnetic anisotropy.[1–4] These clusters with optimized coercive properties, and the extended nanostructures derived from them, should allow the storage of bits on an always smaller number of particles until the ultimate goal of bit storage on a single cluster with the smallest possible size is achieved at room temperature.

Experimental and theoretical studies on metallic clusters of the 3d transition metals, such as iron, cobalt, and nickel, have shown that a decrease in the size of the system results quite generally in an enhancement of spin moments, orbital moments, and magnetic anisotropy energy per atom.[5,6] However, despite this enhancement with respect to the bulk solid, the relatively weak spin–orbit coupling in the 3d elements still yields magnetic anisotropy energies that are far too small and that do not allow room-temperature blocking of magnetic moments on the nanoscale. On the other hand, the heavier 4d and 5d transition metals have a stronger spin–orbit coupling but are usually nonmagnetic as solids or

[a] A. Naitabdi, Dr. O. Toulemonde, Prof. J. P. Bucher, Dr. M. Drillon
Institut de Physique et Chimie des Matériaux de Strasbourg
(UMR 7504 CNRS) Université Louis Pasteur
23 rue du Loess, 67037 Strasbourg (France)
Fax: (+33) 388-107-246
E-mail: Jean-Pierre.Bucher@ipcms.u-strasbg.fr

[b] Dr. J. Rosé, Dr. P. Braunstein
Laboratoire de Chimie de Coordination
Institut de Chimie (UMR 7177 CNRS)
Université Louis Pasteur
4 rue Blaise Pascal, 67070 Strasbourg Cedex (France)
Fax: (+33) 390-241-322
E-mail: braunstein@chimie.u-strasbg.fr

[c] Prof. R. Welter
Laboratoire DECOMET, Institut de Chimie (UMR 7177 CNRS)
Université Louis Pasteur
4 rue Blaise Pascal, 67070 Strasbourg Cedex (France)

nanoparticles. One of the basic innovations in recent years consists of combining 3d and 4d elements to take advantage of the qualities of both, that is, the high moments of 3d elements such as Co, Ni, and Fe and the large spin–orbit coupling of the nonmagnetic 4d elements.[2,4] Although in binary 3d–4d clusters the electronic states are metallic-like, namely, delocalized throughout the particle,[2] these clusters are known for their large magnetic anisotropy energy which leads to an increase in the blocking temperature of small clusters. Furthermore, the electronic structure of ligand-stabilized and naked-metal clusters and the structure and morphology of supported metal particles are very actively studied.[7–9]

Achieving a well-defined stoichiometry of the constituents is a critical issue in the synthesis of alloy clusters and metal thin films. This concept is well known in ultra-high-vacuum (UHV) surface physics, in which evaporator calibration is often a cumbersome task. With the exception of silver and gold nanoalloys,[10] transition-metal nanoalloys have been synthesized only in very limited cases,[11,12] and mixtures of monometallic, carbonyl complexes have typically been used,[13,14] which renders precise control of their composition more difficult than if bimetallic single-source precursors were used. Therefore, new strategies are desirable and the present approach is based on recent advances in both coordination chemistry and surface physics for the fabrication of self-organized bimetallic clusters on surfaces. The approach described herein takes advantage of the ability of molecular chemistry to provide mixed-metal organometallic clusters with a large diversity of core structures and compositions and a perfectly known proportion of the transition-metal atoms A and B they contain.[15,16] To recover the metal components in a form suitable for our purpose, the ligands will be stripped off by thermal treatment after the molecular self-assembling process has taken place on the desired support. This approach has been used for the preparation of cluster-derived bimetallic particles endowed with unique properties in heterogeneous catalysis.[17–20] Tetrahedral A_xB_{4-x} carbonyl clusters ($x=0$—4) form an interesting family of precursors in which the metal centers are already in a low oxidation state, and we focus herein on $\{RuCo_3\}$ carbonyl clusters because of the potentially excellent magnetic anisotropy properties of this alloy. Such clusters have been previously used to generate nanoparticles within mesoporous silica supports, and these were shown to display interesting magnetic properties.[21,22]

Mixed-metal thin films have been obtained from molecular precursors through a metal–organic deposition process on, for example, silicon or glasses,[23,24] and the thermal decomposition of molecular precursors on metal surfaces has been previously performed with the homometallic cluster $[Ru_3(CO)_{12}]$ on Co[25] or Au(111)[26] surfaces deposited under UHV conditions. However, the present investigation describes the formation of a bimetallic deposit on a gold surface obtained by chemical anchoring followed by thermal treatment. The study of the deposition of organometallic molecules on a metal surface is further motivated by the increasing use of such systems in catalytic processes and as a surface-modification method.[25–28] By analogy with the available diverse methods for the functionalization of molecular clusters,[29–31] which allow strong binding to inorganic supports and a high dispersion of the metal particles generated by thermal treatment, functionalization methods are required for a more selective self-organization of organometallic molecules on metal surfaces. This approach is important in itself since this grafting technique represents a promising way toward the assembly of monolayers of molecules on metal surfaces.[32–34]

Results and Discussion

To provide chemical anchoring of the desired, mixed-metal carbonyl cluster onto the gold substrate, one of the carbonyl ligands of the precursor cluster $[RuCo_3(H)(CO)_{12}]$ was substituted by a thiol-containing ligand. This chemical function has the well-known ability to covalently bind to such a surface.[35–38] Owing to its high reactivity (see the Experimental Section), the tetrahedral cluster $[RuCo_3(H)(CO)_{11}(Ph_2PCH_2CH_2SH)]$ (**1**) was obtained in low yield from the reaction of $[RuCo_3(H)(CO)_{12}]$ with $Ph_2PCH_2CH_2SH$ in dichloromethane at room temperature. The molecular structure of **1** was determined by X-ray diffraction studies and is shown in Figure 1.

The carbonyl substitution reaction retains the basic tetrahedral cluster core and the Co–Ru and Co–Co lengths are in the range found for these bonds in related molecules.[39–41] Substitution of one cobalt-bound carbonyl group by the phosphine ligand occurs in the *trans* position with respect to the ruthenium cap, in agreement with previously established

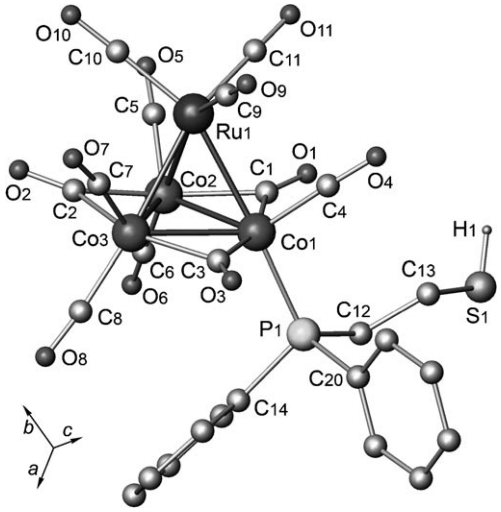

Figure 1. View of the molecular structure of $[RuCo_3(CO)_{11}(H)(Ph_2PCH_2CH_2SH)]$ (**1**). Selected bond lengths [Å] and angles [°]: Ru1–Co1 2.6304(7), Ru1–Co2 2.6373(6), Ru1–Co3 2.6197(8), Co1–Co2 2.5148(7), Co1–Co3 2.5221(9), Co2–Co3 2.5082(9), Co1–P1 2.236(2), P1–C12 1.843(5), C12–C13 1.541(7), S1–C13 1.814(6); Ru1-Co1-P1 174.99(4), Co1-P1-C12 114.8(2), P1-C12-C13 111.8(3), C12-C13-S1 111.4(3).

reactivity patterns.[39,42–44] The axial orientation of the functional phosphine ligand is comparable to the situation in $[RuCo_3(H)(CO)_{11}(PPh_3)]$.[40] The Co–P length of 2.236(2) Å is similar to the values of 2.223(8) and 2.228(2) Å found in $[RuCo_3(CO)_{11}(H)(PMe_3)]$ and $[RuCo_3(CO)_{11}(H)(PMe_2Ph)]$,[41] respectively, but slightly shorter than the value of 2.261(5) Å found in $[RuCo_3(CO)_{11}(H)(PPh_3)]$.[40] The hydride ligand could not be located in X-ray diffraction studies but the ^{1}H NMR chemical shift of $\delta = -20.17$ ppm is consistent with capping of the Co_3 face.[39]

Separation of the reaction mixture, which leads to **1** after column chromatography, also afforded product **2**, which was recrystallized and identified by X-ray diffraction studies as resulting from the intermolecular oxidative coupling of two thiol functions to form a sulfur–sulfur disulfide linkage (Figure 2). Complex **2** is thus constituted by two tetranuclear cluster units linked together by the resulting diphosphine ligand. Each of these cluster units is very similar to **1** and the structure will, therefore, not be discussed in detail. This octanuclear complex is, however, very interesting because its formation results selectively in the diphosphine ligand behaving as a bridge between the clusters, whereas when a long-chain diphosphine ligand is treated with substitutionally labile clusters, complex reactions may result with the possible occurrence of bridging and chelating bonding modes of the ligand. Another point of interest in the context of this study is that disulfide bridges are known to react cleanly with gold surfaces and open to give rise to two Au–S bonds.[45–54]

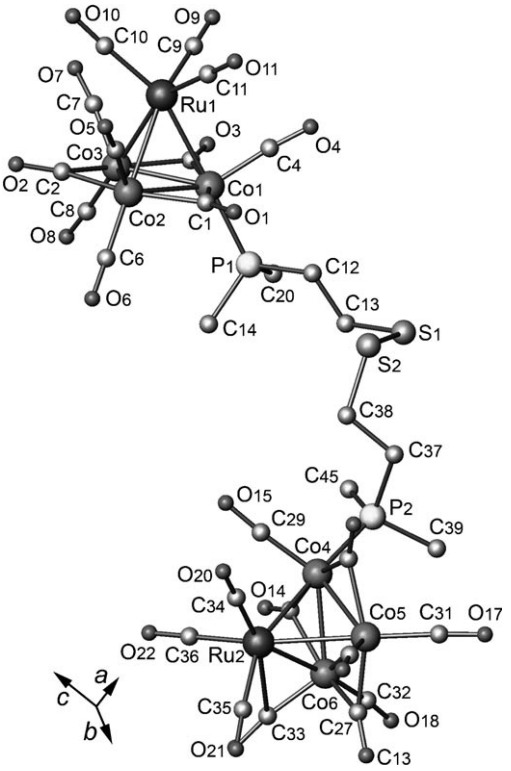

Figure 2. View of the molecular structure of dicluster complex $[\{RuCo_3(CO)_{11}(H)(Ph_2PCH_2CH_2S)\}_2]$ (**2**). Selected bond lengths [Å] and angles [°]: Ru1–Co1 2.629(2), Ru1–Co2 2.645(2), Ru1–Co3 2.642(2), Co1–Co2 2.500(2), Co2–Co3 2.496(2), Co1–Co3 2.507(2), Co1–P1 2.219(2), Ru2–Co4 2.625(2), Ru2–Co5 2.646(2), Ru2–Co6 2.631(1), Co4–Co5 2.514(2), Co5–Co6 2.491(2), Co4–Co6 2.527(2), Co4–P2 2.227(2), S1–S2 2.036(2); Ru1-Co1-P1 176.28(4), Ru2-Co4-P2 175.58(4).

The grafting of the thiol-functionalized cluster **1** by self-assembly was then performed on a Au(111) surface. It is important to emphasize that the clusters exhibit diamagnetic behavior at this stage. Only after the decarbonylation process will the clusters become metallic and exhibit ferromagnetic behavior.

A freshly annealed gold substrate free from organic contaminants was immersed into a 17 μM solution of cluster **1** in dichloromethane for 24 h. During this time, a self-assembled monolayer of cluster molecules forms on the Au(111) surface with breaking of the S–H bond and its replacement with a covalent sulfur–gold linkage. The sample was then rinsed thoroughly with dichloromethane to eliminate any nonanchored material (weakly adsorbed, physisorbed clusters) and dried by exposure to a vigorous flow of pure nitrogen just before characterization.

The characterization of the self-assembled layer was first performed with a scanning tunneling microscope (STM) under UHV conditions at room temperature (pressure was in the range of 10^{-11} mbar). The STM images in Figure 3b,c show that the grafting led to a high coverage of cluster molecules on large Au(111) terraces.

As expected because of the privileged interaction of the clusters with the Au(111) surface, no second layer of clusters was observed. Furthermore, the clusters are found to assemble into organized islands of about 10 nm of lateral exten-

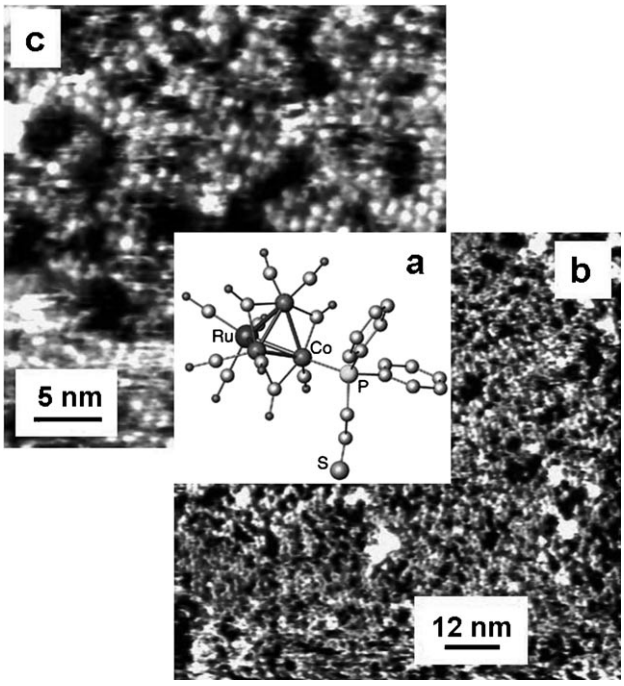

Figure 3. a) View of the molecular structure of $[RuCo_3(CO)_{11}(H)(Ph_2PCH_2CH_2SH)]$ (**1**). b) STM image ($U = 0.3$ V, $I = 40$ pA) of self-assembled cluster molecules of **1** on a Au(111)/mica substrate. c) Close-up view of (b).

sion. The absence of long-range ordering is not surprising since these clusters were not designed to interact laterally through intermolecular links. Moreover, Figure 3b,c shows that the regions between the close-packed patches appear to be free of molecules. These unoccupied zones most probably coincide with the depressions in the gold surface induced by the self-assembly process. Similar defects have been observed previously by STM after the self-assembly of alkane—thiol compounds on Au(111) surfaces.[55] The brightest features in the STM images express the contribution to the tunneling current that come from the overlap of the density of state that arises from the individual atoms (i.e., Co, Ru). Since the tetrahedral metallic structure is not in close contact with the Au(111) surface, the current most probably flows from the gold atoms through the phosphine–thiolate ligand. From the STM image in Figure 3c and the locally ordered molecular arrangement, the dimension of an individual molecule can be estimated to be 1.1 nm. A schematic, scaled view of the possible arrangement of the tetrahedral clusters on the Au(111) surface is shown in Figure 4.

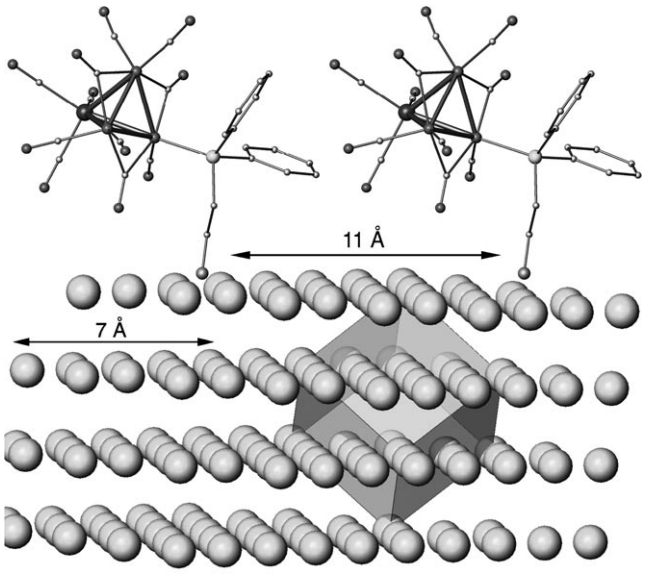

Figure 4. Schematic representation of the interaction between the functional clusters and the Au(111) surface.

Controlled thermal annealing of the self-assembled molecules was then performed to decarbonylate the cluster molecules and obtain metallic products containing cobalt and ruthenium centers in the 3:1 ratio originally present in the molecular cluster. This process was performed under UHV conditions, and the evolution of the chemical state of the elements was monitored by X-ray photoelectron spectroscopy (XPS). The XPS spectra were collected using a VSW X-ray photoelectron spectrometer equipped with a monochromatic $Al_{K\alpha}$ X-ray source ($h\nu = 1486.6$ eV) incident at 45° relative to the axis of the hemispherical analyzer. The base pressure in the chamber during measurements was 2×10^{-10} mbar. The binding energies were referenced by setting the $Au4f_{7/2}$ binding energy to 84 eV. The first XPS measurements were performed at room temperature after self-assembly and prior to thermal annealing. Figure 5 shows the evolution of the XPS spectra of the Co2p line in the $\{RuCo_3\}$ molecules just after self-assembly at 300 K and up to 560 K.

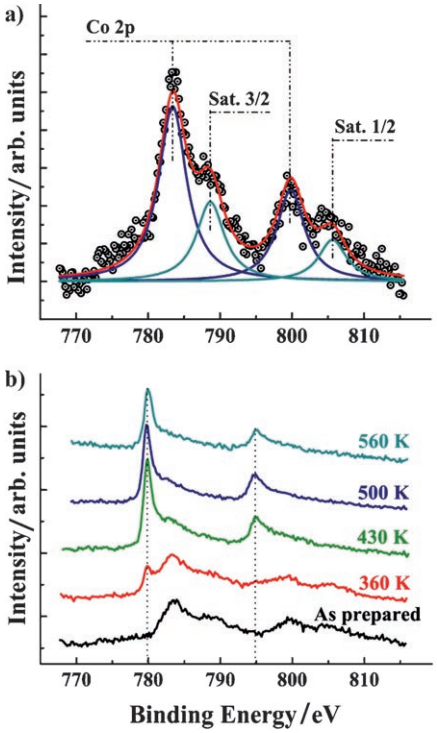

Figure 5. Co2p XPS spectra of a) the species just after self-assembly including the corresponding fits and b) the evolution of the Co2p peaks as a result of increasingly higher annealing temperatures.

The curve at 300 K provides the binding energies of the two peaks $Co2p_{1/2}$ and $Co2p_{3/2}$ at 799.45 and 783.25 eV, respectively. The two values are at least 5 eV above those obtained for pure metallic cobalt. Moreover, the appearance of two shake-up satellites near the main peaks expresses the nonmetallic behavior of the cobalt centers in the monolayer after self-assembly. This finding is expected since, at this stage, the cobalt atoms are still surrounded by carbonyl ligands and the cluster is molecularly adsorbed on the Au(111) surface. The binding energy of $Co2p_{3/2}$ is also larger than the value obtained in the case of isolated {CoO} units (780.2 eV), which rules out the presence of naked cobalt atoms on the surface after self-assembly. The large value of the binding energy can then be ascribed to the Co–carbonyl bonds and to the contribution from the Co–Ru bonds. These indications provide evidence for the retention of the molecular nature of the cluster after the grafting process. In the fitting curve of Co2p at 300 K (Figure 5a), the contribution from the two satellites has been introduced and a spin–orbit coupling of 16.7 eV has been deduced. This value is large compared to that observed for the {CoO} units, thus

indicating the large contribution from the cobalt-bound carbonyl moieties.

Shifts in the XPS spectra of the cobalt centers were observed upon progressive annealing. The evolution of the binding energy expresses the modification of the chemical nature of the molecules as a result of thermal annealing. The spectra were collected after the substrate was cooled down to 300 K. A new peak for $Co2p_{3/2}$ appears at 779.8 eV as a result of annealing to 360 K over 90 minutes (Figure 5b). This process also induced a noticeable decrease in the intensities of the two satellites, mainly for the satellite at the lower binding energy. The line for $Co2p_{3/2}$ at 779.8 eV corresponds to the binding energy of elemental cobalt. This behavior expresses the evolution of the cobalt center in the $\{Co_3Ru\}$ unit toward a metallic behavior and points toward the onset of the loss of the carbonyl moieties. At this stage, however, the contribution from the carbonyl ligands is still significant and most of the cobalt centers remain in their initial state. The next heating step to 430 K over 60 minutes induces major changes in the XPS spectra of the cobalt centers. The significant shift of the peak for $Co2p_{1/2}$ toward lower binding energies and the fading of the contribution from the absorption for $Co2p_{3/2}$ at higher energy (783.25 eV, Co–carbonyl) provide clear evidence for the loss of the carbonyl ligands and confirm the tendency toward the formation of metallic cobalt.

Upon annealing to 500 K, the contribution from $Co2p_{3/2}$ (at 783.25 eV) disappears, thus confirming complete loss of the carbonyl ligands. The unchanged values of the binding energies of $Co2p_{3/2}$ and $Co2p_{1/2}$ at 779.8 and 794.7 eV, respectively, after annealing from 430 to 560 K are indicative of the stabilization of metallic cobalt. However, a noticeable decrease in the intensity of the cobalt was observed after the last annealing process up to 560 K, which corresponds to a Co/Ru ratio of only 1:1. This behavior can be attributed to the tendency of the cobalt atoms to sink into the gold substrate, as previously observed in the case of self-organized cobalt aggregates on a Au(111) surface.[56] Consequently, retention of the stoichiometry of the $\{RuCo_3\}$ unit at the surface cannot be guaranteed above 560 K. Further characterization of the decarbonylation process in the self-assembled monolayer of $\{RuCo_3\}$ clusters may be achieved using the XPS curves of Ru3d. The evolution of the peaks for Ru3d is shown in Figure 6.

The XPS curves shown in Figure 6 provide information on the chemical state of the ruthenium centers in the cluster molecules after self-assembling on a Au(111) surface and as a function of the annealing temperature. After self-assembly of the molecular clusters **1** (but before heating), the binding energies of $Ru3d_{5/2}$ and $Ru3d_{3/2}$ are 283.1 and 286.7 eV, respectively. Again, the large binding energies of Ru3d, namely +4 eV with respect to the bulk metallic Ru, point to a large contribution from the ruthenium-bound carbonyl ligands. The fitting of the signal for Ru3d in Figure 6 also provides accurate contributions from carbon monoxide and elemental carbon. The significant amount of carbon monoxide is attributed to the carbonyl ligands. Although the presence

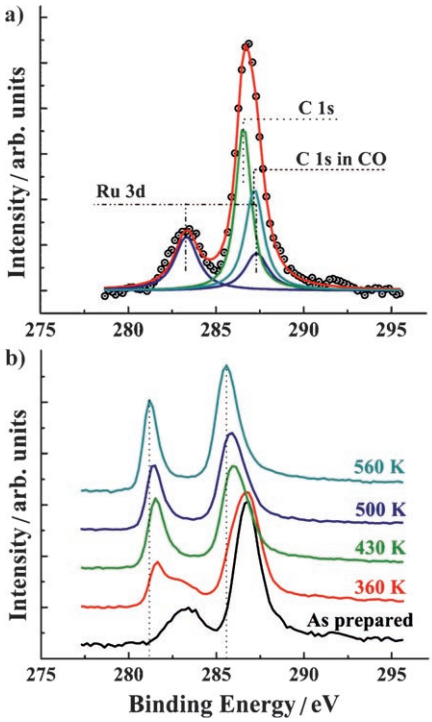

Figure 6. Ru3d XPS spectra of a) species just after self-assembly including the corresponding fits and b) the evolution of the Ru3d peaks as a result of increasingly higher annealing temperatures.

of 14 carbon atoms in the phosphine–thiolate unit of the $\{RuCo_3\}$ cluster molecule contributes to the XPS carbon signal, it does not account for all of the carbon present on the surface. The remaining quantity of carbon should mainly be a result of contamination since the sample was prepared ex situ before introduction into the UHV chamber. Using the fitting parameters and on the basis of the integral peak intensities and atomic sensitivity factors, the relative concentration of ruthenium, cobalt, carbon monoxide, and carbon provides the formulation $[RuCo_{2.8}(CO)_{10}(Csp^3 \text{ and } Csp^2)_{13.5}]$, which is very close to the expected stoichiometry of the molecules $[RuCo_3(CO)_{11}(Csp^3 \text{ and } Csp^2)_{14}]$ after their self-assembly. The first modification in the chemical state of the ruthenium centers is visible after annealing at 360 K. The increase of the peak for Ru3d at lower energy (281.5 eV) is the result of a partial loss of carbonyl ligands and can be attributed to the ruthenium centers that are bound to some residual carbonyl ligands. The progressive shifts of the peak for Ru3d toward lower binding energies, as a result of heating from 360 to 560 K, is an additional interesting feature. This behavior corresponds to the progressive shift of ruthenium towards a metallic state, as a result of the gradual loss of the carbonyl ligands.

Retention of the stoichiometry of cobalt and ruthenium was monitored after each annealing step. For this purpose, the intensity of a given element X, measured from the XPS data, must be corrected for the atomic sensitivity factor: $I_X = I_{meas}/\sigma\lambda$, where I_{meas} corresponds to the integrated intensity calculated from the XPS peak area, σ is the cross-sec-

tion, and λ is the mean free path ($\lambda = 0.54\sqrt{E_C}$). The chemical composition of the deposit was calculated and is represented in Figure 7 as a function of the annealing temperature. It is shown that the chemical composition of the deposit becomes stable for annealing temperatures above 400 K. The calculation leads to $I_{Co}/I_{Ru} = 3.0$, which is in good agreement with the expected, unperturbed stoichiometric composition of the $\{RuCo_3\}$ particles in the metallic state. It can be noticed that the annealing process also leads to the loss of phosphorus, thus preventing contamination of the exposed metallic $\{RuCo_3\}$ clusters after decarbonylation.

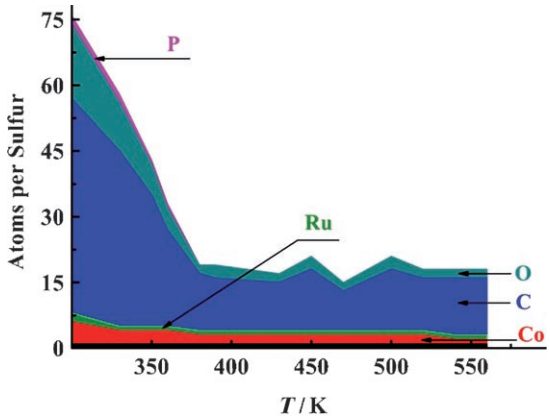

Figure 7. The atomic composition of the self-assembled $\{RuCo_3\}$ layer after annealing treatments from 300 to 600 K.

It was not possible to examine the metallic deposit by STM after stripping away the ligands. Indeed STM and XPS measurements are performed in different UHV chambers and transferring the sample from the XPS chamber into the STM chamber would result in oxidation of the fragile metallic structures during the passage at ambient atmosphere. It is to be expected, however, that Co–Ru metal islands are formed on the gold surface. Assuming that a four-metal-atom cluster occupies an area of approximately 1.2 nm^2 (Figures 3 and 4), about 30% of the Au(111) surface is covered by the cobalt and ruthenium atoms after thermal stripping. If the islands nucleate at the elbows of the surface reconstruction of the Au(111) surface, which seems to be a reasonable assumption,[57] one would expect them to contain 370 atoms on average, each island thus occupying a rectangular unit cell of 15×7.5 nm^2.

Preliminary results of XAS investigations on synchrotron starting from **2** are identical to those with **1**, which is consistent with the breaking of the disulfide linkage to give two Au–S bonds.[45–54] This finding appears to be promising since the former precursor is easier to prepare and is more stable than **1**. Future investigations will focus on the use of **2** and on more detailed comparisons between these precursors.

Conclusion

The technique presented herein provides a good alternative to physical vapor deposition for the formation of metallic clusters or thin-film alloys. The feasibility of the two-step process, namely, grafting of the molecular precursor and stripping away the ligands under UHV conditions, has been demonstrated. The observed behavior clearly indicates that the deposit retains the bimetallic stoichiometry of the precursor cluster, thus making the technique suitable for the study of the influence of alloying on the improvement of magnetic properties. Element-specific X-ray magnetic circular dichroism (XMCD) measurements are underway to study the paramagnetic nature of the metallic-cluster products, also to follow the onset of cluster magnetism as a function of the annealing temperature. Molecular precursors such as those investigated herein also represent interesting model systems to study the interaction between molecules and metal surfaces on the atomic scale, which is highly relevant to the development of functional molecular electronics.

Experimental Section

General: All manipulations were carried out under an inert dinitrogen atmosphere and used standard Schlenk-line techniques and dried, freshly distilled solvents. The ^1H, $^{31}P\{^1H\}$, and ^{59}Co NMR spectra were recorded at 298 K on a Bruker Avance 400 instrument at 400.13, 161.97, and 94.7 MHz, respectively, using trimethylsilane, H_3PO_4 (85% in D_2O), or $[K_3Co(CN)_6]$ in D_2O as external standards with downfield shifts reported as positive. The compounds $[RuCo_3(H)(CO)_{12}]$[44] and (diphenylphosphino)ethanethiol $(Ph_2PCH_2CH_2SH)$[58] were prepared according to literature procedures.

The XPS spectra were collected using a VSW X-ray photoelectron spectrometer equipped with a monochromatic $Al_{K\alpha}$ X-ray source ($h\nu$ = 1486.6 eV) incident at 45° relative to the axis of the hemispherical analyzer. The base pressure in the chamber during measurements was 2×10^{-10} mbar. The binding-energy values were referenced by setting the $Au4f_{7/2}$ binding energy to 84 eV. The samples were examined over a large temperature range of 300–560 K.

For STM measurements, the self-assembled layers were introduced in the UHV equipment through a fast-load lock and were studied without further treatment in a modified commercial UHV–STM from Omicron at room temperature (pressure in the range of 10^{-10} mbar).

Preparation of $[RuCo_3(CO)_{11}(H)(Ph_2PCH_2CH_2SH)]$ (1) and $[\{RuCo_3(CO)_{11}(H)(Ph_2PCH_2CH_2S)\}_2]$ (2): The pure ligand (diphenylphosphino)ethanethiol (0.250 mL, 1.140 mmol) was added slowly to a solution of $[RuCo_3(H)(CO)_{12}]$ (0.700 g, 1.140 mmol) in CH_2Cl_2 (50 mL), and the wine-red reaction mixture immediately turned dark red and was stirred at room temperature. The reaction mixture was monitored by TLC, which indicated the formation of the major product **1** together with other minor compounds. After the reaction mixture was stirred for 0.25 h, the dark red solution was filtered and purified by chromatography over silica gel using hexane/CH_2Cl_2 (80:20) as the eluant, which afforded three main bands. The first, fast-moving red band of residual $[RuCo_3(H)(CO)_{12}]$ was followed by a second red band of pure **1** (0.050 g, 6%). ^1H NMR (400.13 MHz, $CDCl_3$): $\delta = -20.17$ (s, 1H, μ_3-H), 1.65 (t, 1H, SH), 2.48 (m, 2H, CH_2P), 2.64 (m, 2H, CH_2S), 7.26–7.49 ppm (m, 10H, Ph); $^{31}P\{^1H\}$ NMR (161.97 MHz, $CDCl_3$): $\delta = 27.25$ ppm (br, $\omega_{1/2} = 1170$ Hz); ^{59}Co NMR (94.7 MHz, $CDCl_3$): $\delta = -2735$ (br, 2Co, $\omega_{1/2} = 5400$ Hz), -2632 ppm (br, 1Co, CoP, $\omega_{1/2} = 4340$ Hz); IR (pentane, ν_{CO}): 2082 m, 2046 s, 2035 s,sh, 2010 s, 1896 w, 1868 m, 1845 m cm^{-1}.

However, cluster **1** was unstable in solution at room temperature and transformed during chromatography, which explains why **1** was the major species found during monitoring of the reaction mixture by TLC but was isolated after column chromatography in low yield. Thus, further elution with hexane/CH_2Cl_2 (70:30) gave another dark-red band, thus affording **2** (0.380 g, 20%). ^1H NMR (400.13 MHz, $CDCl_3$): $\delta = -20.15$ (s, 1H, μ_3-H),

2.47 (m, 2H, CH_2P), 2.70 (m, 2H, CH_2S), 7.17–7.45 ppm (m, 10H, Ph); $^{31}P\{^1H\}$ NMR (161.97 MHz, $CDCl_3$): $\delta = 26.22$ ppm (br, $\omega_{1/2} = 1100$ Hz); ^{59}Co NMR (94.7 MHz, $CDCl_3$): $\delta = -2724$ (br, 2Co, $\omega_{1/2} = 7100$ Hz), -2628 ppm (br, 1Co, CoP, $\omega_{1/2} = 6600$ Hz); IR (pentane, ν_{CO}): 2082m, 2046s, 2035s,sh, 2010s, 1896w, 1868m, 1845m cm^{-1}.

X-ray diffraction studies: Selected crystals were mounted on a Nonius Kappa-CCD area detector diffractometer ($Mo_{K\alpha}$, $\lambda = 0.71073$ Å). The complete conditions under which the data collection (Denzo software) and structure refinements were carried out are given in the corresponding cif files. The cell parameters were determined from reflections taken from one set of ten frames (1.0° steps in phi angle), each at 20-s exposure. The structures were solved using direct methods (SHELXS97) and refined against *I* by using the SHELXL97 software. All the non-hydrogen atoms were refined anisotropically. Hydrogen atoms were generated according to stereochemistry and refined using a riding model in SHELXL97.

CCDC 670990 and 970991 contain the supplementary crystallographic data for this paper. These data can be obtained free of charge from the Cambridge Crystallographic Data Centre via www.ccdc.cam.ac.uk/data_request/cif.

Acknowledgements

We thank J. Hommet for helpful discussion on the interpretation of the XPS data. We are grateful to the Centre National de la Recherche Scientifique, the Ministère de la Recherche (ACI 2001 ORGANOMETMAG), and the ULP (Appel du Conseil Scientifique 2001) for financial support.

[1] E. O. Berlanga-Ramirez, F. Aguiler-Granja, J. M. Montejano-Carrizales, A. Diaz-Ortiz, K. Michaelian, A. Vega, *Phys. Rev. B* **2004**, 14410.
[2] S. Dennler, J. Morillo, G. M. Pastor, *J. Phys. Condens. Matter* **2004**, *16*, S2263.
[3] T. Sondon, J. Guevara, A. Saul, *Phys. Rev. B* **2007**, 104426.
[4] D. Zitoun, M. Respaud, M. C. Fromen, M. J. Casanove, P. Lecante, C. Amiens, B. Chaudret, *Phys. Rev. Lett.* **2002**, *89*, 37203.
[5] J. Dorantes-Davila, H. Dreyssé, G. M. Pastor, *Phys. Rev. Lett.* **2003**, *91*, 197206.
[6] R. Guirado-Lopez, J. Dorantes-Davila, G. M. Pastor, *Phys. Rev. Lett.* **2003**, *90*, 226402.
[7] N. Rösch, G. Pacchioni, in *Clusters and Colloids, from Theory to Applications* (Ed.: G. Schmid), Wiley-VCH, Weinheim, **1994**.
[8] *Metal Clusters in Chemistry, Vol. 3* (Eds: P. Braunstein, L. A. Oro, P. R. Raithby), Wiley-VCH, Weinheim, **1999**.
[9] G. Schmid, U. Simon, *Chem. Commun.* **2005**, 697.
[10] C. J. Kiely, J. Fink, J. G. Zheng, M. Brust, D. Bethell, D. J. Schiffrin, *Adv. Mater.* **2000**, *12*, 640.
[11] Y. Yamada, T. Suzuki, E. N. Abarra, *IEEE Trans. Magn.* **1998**, *34*, 343.
[12] M. Thielen, S. Kirsch, A. Weinforth, A. Carl, E. F. Wassermann, *IEEE Trans. Magn.* **1998**, *34*, 1009.
[13] M. Zubris, R. B. King, H. Garmestani, R. Tannenbaum, *J. Mater. Chem.* **2005**, *15*, 1277.
[14] K. E. Gonsalves, H. Li, R. Perez, P. Santiago, M. Jose-Yacaman, *Coord. Chem. Rev.* **2000**, *206–207*, 607.
[15] *Metal Clusters in Chemistry, Vol. 1–3* (Eds: P. Braunstein, L. A. Oro, P. R. Raithby), Wiley-VCH, Weinheim, **1999**.
[16] *Clusters and Colloids, from Theory to Applications* (Ed.: G. Schmid), Wiley-VCH, Weinheim, **1994**.
[17] P. Braunstein, R. Bender, J. Kervennal, *Organometallics* **1982**, *1*, 1236.
[18] P. Braunstein, J. Kervennal, J.-L. Richert, *Angew. Chem.* **1985**, *97*, 762; *Angew. Chem. Int. Ed. Engl.* **1985**, *24*, 768.
[19] P. Braunstein, J. Rosé, in *Metal Clusters in Chemistry, Vol. 2* (Eds.: P. Braunstein, L. A. Oro, P. R. Raithby), Wiley-VCH, Weinheim, **1999**, p. 616.
[20] S. Hermans, T. Khimyak, R. Raja, G. Sankar, J. M. Thomas, B. F. G. Johnson, in *Nanotechnology in Catalysis* (Eds.: B. Zhou, S. Hermans, G. A. Somorjai), Kluwer Academic, Plenum Publishers, New York, **2004**.
[21] F. Schweyer, P. Braunstein, C. Estournès, J. Guille, H. Kessler, J.-L. Paillaud, J. Rosé, *Chem. Commun.* **2000**, 1271.
[22] F. Schweyer, P. Braunstein, C. Estournès, J. Guille, J.-L. Paillaud, M. Richard-Plouet, J. Rosé, *Phys. Chem. Chem. Phys.* **2006**, *8*, 4018.
[23] N. Auvray, P. Braunstein, S. Mathur, M. Veith, H. Shen, S. Hüfner, *New J. Chem.* **2003**, *27*, 155.
[24] E. P. Boyd, D. R. Ketchum, H. Deng, S. G. Shore, *Chem. Mater.* **1997**, *9*, 1154.
[25] J. Vaari, J. Lahtinen, P. Hautojärvi, *Surf. Sci.* **1996**, *346*, 11.
[26] T. Cai, Z. Song, Z. Chang, G. Liu, J. A. Rodriguez, J. Hrbek, *Surf. Sci.* **2003**, *538*, 76.
[27] A. M. Argo, J. F. Odzak, F. S. Lai, B. C. Gates, *Nature* **2002**, *415*, 623.
[28] R. Psaro, S. Recchia, *Catal. Today* **1998**, *41*, 139.
[29] P. Braunstein, *J. Organomet. Chem.* **2004**, *689*, 3953.
[30] A. Choualeb, J. Rosé, P. Braunstein, R. Welter, *Organometallics* **2003**, *22*, 2688.
[31] F. Schweyer-Tihay, P. Braunstein, C. Estournès, J. L. Guille, B. Lebeau, J.-L. Paillaud, M. Richard-Plouet, J. Rosé, *Chem. Mater.* **2003**, *15*, 57.
[32] A. Naitabdi, J. P. Bucher, P. Gerbier, P. Rabu, M. Drillon, *Adv. Mater.* **2005**, *17*, 1612.
[33] L. Ramoino, M. von Arx, S. Schintke, A. Baratoff, H.-J. Güntherodt, T. A. Jung, *Chem. Phys. Lett.* **2006**, *417*, 22.
[34] G. Schmid, M. Bäumle, N. Beyer, *Angew. Chem.* **2000**, *112*, 187; *Angew. Chem. Int. Ed.* **2000**, *39*, 181.
[35] Y.-T. Kim, R. L. McCarley, A. J. Bard, *J. Phys. Chem.* **1992**, *96*, 7416.
[36] F. Ragaini, L. Lunardi, D. Tomasoni, V. Guglielmi, *J. Organomet. Chem.* **2004**, *689*, 3621.
[37] J. A. Rodriguez, J. Dvorak, T. Jirsak, G. Liu, J. Hrbek, Y. Aray, C. Gonzalez, *J. Am. Chem. Soc.* **2003**, *125*, 276.
[38] J. I. Henderson, S. Feng, G. M. Ferrence, T. Bein, C. P. Kubiak, *Inorg. Chim. Acta* **1996**, *242*, 115.
[39] P. Braunstein, L. Mourey, J. Rosé, P. Granger, T. Richert, F. Balegroune, D. Grandjean, *Organometallics* **1992**, *11*, 2628.
[40] H. Matsuzaka, T. Kodama, Y. Uchida, M. Hidai, *Organometallics* **1988**, *7*, 1608.
[41] J. Pursiainen, M. Ahlgren, T. A. Pakkanen, J. Valkonen, *J. Chem. Soc. Dalton Trans.* **1990**, 1147.
[42] P. Braunstein, J. Rosé, D. Toussaint, S. Jääskeläinen, M. Ahlgren, T. A. Pakkanen, J. Pursiainen, L. Toupet, D. Grandjean, *Organometallics* **1994**, *13*, 2472.
[43] S. Bouherour, P. Braunstein, J. Rosé, L. Toupet, *Organometallics* **1999**, *18*, 4908.
[44] P. Braunstein, J. Rosé, P. Granger, J. Raya, S.-E. Bouaoud, D. Grandjean, *Organometallics* **1991**, *10*, 3686.
[45] H. A. Biebuyck, C. D. Bain, G. M. Whitesides, *Langmuir* **1994**, *10*, 1825.
[46] M. T. Rojas, A. E. Kaifer, *J. Am. Chem. Soc.* **1995**, *117*, 5883.
[47] A. Ulman, *Chem. Rev.* **1996**, *96*, 1533.
[48] T. Ishida, S. Yamamoto, W. Mizutani, M. Motomatsu, H. Tokumoto, H. Hokari, H. Azehara, M. Fujihira, *Langmuir* **1997**, *13*, 3261.
[49] J. Noh, M. Hara, *Langmuir* **2000**, *16*, 2045.
[50] S. Yoshimoto, N. Hirakawa, K. Nishiyama, I. Taniguchi, *Langmuir* **2000**, *16*, 4399.
[51] M. S. Boeckl, A. L. Bramblett, K. D. Hauch, T. Sasaki, B. D. Ratner, J. W. Rogers Jr., *Langmuir* **2000**, *16*, 5644.
[52] H. Grönbeck, A. Curioni, W. Andreoni, *J. Am. Chem. Soc.* **2000**, *122*, 3839.
[53] N. Weber, C. Hamann, J.-M. Kern, J.-P. Sauvage, *Inorg. Chem.* **2003**, *42*, 6780.
[54] T. Belser, M. Stöhr, A. Pfaltz, *J. Am. Chem. Soc.* **2005**, *127*, 8720.

[55] S. Padovani, F. Scheurer, J. P. Bucher, *Europhys. Lett.* **1999**, *45*, 327.
[56] J. P. Bucher, L. Santesson, K. Kern, *Langmuir* **1994**, *10*, 979.
[57] I. Chado, C. Goyhenex, H. Bulou, J. P. Bucher, *Phys. Rev. B* **2004**, *69*, 085413.
[58] J. Chatt, J. R. Dilworth, J. A. Schmutz, J. A. Zubieta, *J. Chem. Soc. Dalton* **1979**, 1595.

Received: September 21, 2007
Published online: January 18, 2008

